

# A Resonance Model for Spontaneous Cortical Activity

Yanjiang Wang<sup>1\*</sup>, Jichao Ma<sup>1</sup>, Jiebin Luo<sup>1</sup>, Xue Chen<sup>2</sup>, Yue Yuan<sup>1</sup>

<sup>1</sup>*College of Control Science and Engineering, China University of Petroleum (East China), Qingdao 266580, P. R. China*

<sup>2</sup>*The Institute for Digital Medicine and Computer-assisted Surgery in Qingdao University, Qingdao University, Qingdao 266071, China*

We propose a resonance model for spontaneous cortical activity, which is able to predict the resting brain functional connectivity (FC) accurately given that the structural connection strength and the sign (excitatory or inhibitory) of each connection are known. The resulting FC fits well with the empirical FC measured with functional magnetic resonance imaging (fMRI), outperforming most of the existing typical models. The proposed model is tested and confirmed with a large cohort of subjects (>1000) from the Human Connectome Project (HCP) S1200 release in both time and frequency domain.

Strong temporal correlations across different distributed brain regions during rest have been observed in spontaneous fluctuations with low frequency (<0.1Hz) measured with fMRI [1]. Yet how such slowly fluctuated and spatio-temporally organized functional patterns, referred to as resting-state functional connectivity (FC), emerge from the underlying structural connectivity (SC) measured with diffusion MRI (dMRI) [2], still remains an open question in neuroscience. Existing network-based models usually regard SC as a fixed connectome or a graph network with its nodes representing brain regions and weighted edges indicating the connection strengths [3-9]. The simulated FC relies mainly on directly connected structural information such as the number of white matter tracts or connection density estimated by diffusion tractography algorithms [10], lacking the ability to describe the higher-order relationship between SC and FC. Whereas neural mass models (NMMs) [11-14] or neural field models [15,16] often suffer from the determination of a number of physiological parameters, leading to the models being less convincing. Therefore, neither network-based models nor neural mass models are able to completely describe the overall pattern of FC. Crucially, none of the models is able to accurately

simulate negative functional correlations due to the inability of dMRI to measure some dynamic structural information such as the causal influences of one region over another or the excitatory and inhibitory interactions between brain regions.

Recently, graph Laplacian and spectral graph analysis bring new insights into understanding the relation between brain structure and function [17-22]. The eigenvectors and eigenvalues of the structural connectome Laplacian, respectively implying the connectome harmonics and the corresponding spatial frequencies have been found to match some of the resting brain network patterns to a certain extent [23-25]. However, the graph Laplacian based connectome harmonics models are also unable to capture the higher-order relations between SC and FC owing to the sparseness of the Laplacian matrix. To remedy this limitation, we proposed a spatiotemporal varying hypergraph Laplacian diffusion model (STV-HGLD) in a recent study [26] by incorporating the higher-order hypergraph Laplacian of SC into the regular wave equation to simulate the dynamic functional correlations, in which a sign matrix indicating the positive and negative correlations is embedded into the hypergraph Laplacian to yield the negative correlations. While the STV-HGLD model can

describe the functional correlations with more accuracy, the underlying biological mechanisms remain elusive.

In fact, studies in neuroscience have evidenced that the self-organizing between synaptic excitation and inhibition plays a dominant role in shaping cortical activity [27]. Notably, resonance may occur to SC during the interplay between the fast local oscillations in gamma frequency range [28]. To this end, in this letter, we present a resonance model to describe the spontaneous cortical activity by incorporating the dynamic interactions between neuronal populations into a wave equation. We find that the low-frequency dynamic couplings between brain regions result from the resonance with the coherent oscillations between brain regions, which fluctuate in the form of Gaussian wave regulated by the harmonics shaped from the interplay between excitation and inhibition arising from the oscillating. Remarkably, the resting-state FC can be theoretically determined from the model and the frequency of the fluctuation yielding the spontaneous cortical wave can be identified as well.

*Dynamic brain network notation.*—The dynamic brain network is defined as  $\mathbf{G}=(\mathbf{V},\mathbf{E},\mathbf{S})$ , where  $\mathbf{V}=\{v_i|i\in 1,2,\cdots,n\}$  represents  $n$  brain regions,  $\mathbf{E}=\{(i,j)|i\in \mathbf{V}, j\in \mathbf{V}\}$  labels the edge linking region  $i$  and  $j$ , whose weight  $w_{i,j}$  measuring the anatomical connection strength between the two regions.  $\mathbf{W}=\{w_{i,j}|(i,j)\in \mathbf{E}\}$  denotes the structural connectivity matrix, and  $\mathbf{S}=\{s_{i,j}|(i,j)\in \mathbf{E}\}$  defines the interplay of excitation and inhibition between region  $i$  and region  $j$ . For simplicity, here we just denote by  $s_{i,j}$  the signs of the connections between the two brain regions after a period of time, with  $s_{i,j}=1$  and  $s_{i,j}=-1$  respectively specifying the excitatory and inhibitory connections. Let  $\mathbf{D}$  denote the degree matrix,  $\mathbf{D}=diag(d_i)$ ,  $d_i=\sum_{j=1}^n w_{i,j}$ , then the graph Laplacian of  $\mathbf{G}$  is defined as  $\mathbf{L}=\mathbf{D}-\mathbf{W}$  and  $\mathbf{L}$  can be decomposed as  $\mathbf{L}=\mathbf{U}\mathbf{A}\mathbf{U}^T$ , where  $\mathbf{U}$  and  $\mathbf{A}$  are the matrices containing the eigenvectors and eigenvalues of  $\mathbf{L}$ , respectively.

*Spontaneous cortical activity modeling.*—Studies in neuroscience show that if a firing neuron causes another neuro to fire, the connection strength between the two neurons will increase otherwise decrease, which is referred to as spike timing dependent plasticity (STDP) [29]. The STDP can be generalized to the macroscale case, i.e., the connection strength between two brain regions will also fluctuate during information exchange between them, suggesting that if the connection between two regions exhibits excitatory behavior, the connection strength will increase, otherwise decrease for an inhibitory connection.

Specifically, supposing  $\mathbf{x}=[x_1, x_2, \cdots, x_n]^T$ ,  $x_i=\mathbf{x}(i, t)$  specifies the cortical activity signal of the  $i$ th brain region at time  $t$ ,  $T$  indicates transpose.

Regarding the theory of STDP and the above brain network notation, the firing of the neurons in the  $j$ th brain region will cause excitatory or inhibitory effect to the  $i$ th brain region, giving rise to a little fluctuation to the weight  $w_{i,j}$  vary with time, i.e.,  $\Delta w_{i,j}(t)$ , which usually varies linearly within a short period of time [30], i.e.,

$$\Delta w_{i,j}(t)=w_{i,j}t \quad (1)$$

Then the total first-order fluctuation on the  $i$ th brain region caused by all the other brain regions linking to it can be expressed as

$$\nabla x_i = \sum_{j\in n} \Delta w_{i,j}(t) (s_{i,j}x_j - x_i) \quad (2)$$

where  $s_{i,j}$  indicates the sign of the connection (excitatory or inhibitory) between region  $i$  and  $j$ . Bring all the regions together, the above first-order dynamics can be described as

$$\begin{aligned} \nabla x_1 &= (w_{1,1}s_{1,1}x_1 + w_{1,2}s_{1,2}x_2 + \cdots + w_{1,n}s_{1,n}x_n) t - (w_{1,1}x_1 + w_{1,2}x_2 + \cdots + w_{1,n}x_n) t \\ \nabla x_2 &= (w_{2,1}s_{2,1}x_1 + w_{2,2}s_{2,2}x_2 + \cdots + w_{2,n}s_{2,n}x_n) t - (w_{2,1}x_2 + w_{2,2}x_2 + \cdots + w_{2,n}x_n) t \\ &\vdots \\ \nabla x_n &= (w_{n,1}s_{n,1}x_1 + w_{n,2}s_{n,2}x_2 + \cdots + w_{n,n}s_{n,n}x_n) t - (w_{n,1}x_n + w_{n,2}x_n + \cdots + w_{n,n}x_n) t \end{aligned} \quad (3)$$

Using matrix notations, Eq. (3) can be rewritten as

$$\begin{aligned}
\nabla \mathbf{x} &= \begin{bmatrix} \nabla x_1 \\ \nabla x_2 \\ \vdots \\ \nabla x_n \end{bmatrix} = \begin{bmatrix} w_{1,1}s_{1,1} & w_{1,2}s_{1,2} & \cdots & w_{1,n}s_{1,n} \\ w_{2,1}s_{2,1} & w_{2,2}s_{2,2} & \cdots & w_{2,n}s_{2,n} \\ \vdots & \vdots & \ddots & \vdots \\ w_{n,1}s_{n,1} & w_{n,2}s_{n,2} & \cdots & w_{n,n}s_{n,n} \end{bmatrix} \begin{bmatrix} x_1 \\ x_2 \\ \vdots \\ x_n \end{bmatrix} t \\
&= \begin{bmatrix} (w_{1,1} + w_{1,2} + \cdots + w_{1,n}) & 0 & \cdots & 0 \\ 0 & (w_{2,1} + w_{2,2} + \cdots + w_{2,n}) & \cdots & 0 \\ 0 & 0 & \cdots & (w_{n,1} + w_{n,2} + \cdots + w_{n,n}) \end{bmatrix} \begin{bmatrix} x_1 \\ x_2 \\ \vdots \\ x_n \end{bmatrix} t \\
&= \begin{bmatrix} w_{1,1} & w_{1,2} & \cdots & w_{1,n} \\ w_{2,1} & w_{2,2} & \cdots & w_{2,n} \\ \vdots & \vdots & \ddots & \vdots \\ w_{n,1} & w_{n,2} & \cdots & w_{n,n} \end{bmatrix} \circ \begin{bmatrix} s_{1,1} & s_{1,2} & \cdots & s_{1,n} \\ s_{2,1} & s_{2,2} & \cdots & s_{2,n} \\ \vdots & \vdots & \ddots & \vdots \\ s_{n,1} & s_{n,2} & \cdots & s_{n,n} \end{bmatrix} \begin{bmatrix} x_1 \\ x_2 \\ \vdots \\ x_n \end{bmatrix} t \\
&- \begin{bmatrix} d_1 & 0 & \cdots & 0 \\ 0 & d_2 & \cdots & 0 \\ \vdots & \vdots & \ddots & \vdots \\ 0 & 0 & \cdots & d_n \end{bmatrix} \begin{bmatrix} x_1 \\ x_2 \\ \vdots \\ x_n \end{bmatrix} t \\
&= (\mathbf{W} \circ \mathbf{S} - \mathbf{D}) t \mathbf{x} = -(\mathbf{D} - \mathbf{W} \circ \mathbf{S}) t \mathbf{x} \quad (4)
\end{aligned}$$

where  $\mathbf{W}$ ,  $\mathbf{D}$ , and  $\mathbf{S}$  denote the adjacency, degree, and the sign matrices respectively, ‘ $\circ$ ’ denotes the Hadamard product. Using the definition of graph Laplacian, here we define  $\mathbf{L}_R = \mathbf{D} - \mathbf{W} \circ \mathbf{S}$  as the resonant Laplacian

Since the sign matrix  $\mathbf{S}$  is equivalent to  $\mathbf{W}_H \circ \mathbf{S}$ , where  $\mathbf{W}_H$  corresponds to an adjacency matrix with all the elements being 1 excluding the diagonal entries, then  $\mathbf{L}_R$  can be rewritten as

$$\mathbf{L}_R = \mathbf{D} - \mathbf{W} \circ \mathbf{W}_H \circ \mathbf{S} \quad (5)$$

Factorizing matrix  $\mathbf{L}_R$  using eigendecomposition, i.e.,  $\mathbf{L}_R = \mathbf{U}_R \mathbf{A}_R \mathbf{U}_R^T$ , where  $\mathbf{U}_R$  consists of eigenfunctions representing the harmonics shaped by the self-organizing interaction between excitation and inhibition (determined by  $\mathbf{W}_H$  and  $\mathbf{S}$ ), while  $\mathbf{A}_R$  contains eigenvalues representing the spatial frequencies corresponding to each harmonic (determined by  $\mathbf{W}$ ).

Applying the  $\nabla$  operator again, we obtain the second-order fluctuation, i.e., the Laplace operator, as follows:

$$\nabla^2 \mathbf{x} = \nabla(\nabla \mathbf{x}) = (-\mathbf{L}_R t)(-\mathbf{L}_R t \mathbf{x}) = \mathbf{L}_R^2 t^2 \mathbf{x} \quad (6)$$

Substituting Eq. (6) into the following regular wave equation:

$$\nabla^2 \mathbf{x} = \frac{1}{\beta^2} \frac{\partial^2 \mathbf{x}}{\partial t^2} \quad (7)$$

where  $\beta$  is the decay factor.

Then we obtain

$$\nabla^2 \mathbf{x} = \mathbf{L}_R^2 t^2 \mathbf{x} = \frac{1}{\beta^2} \frac{\partial^2 \mathbf{x}}{\partial t^2} \quad (8)$$

Equation (8) has an explicit solution (see SI for the proof)

$$\mathbf{x} = k e^{-\frac{1}{2} \beta \mathbf{L}_R t^2} \quad (9)$$

Applying the eigendecomposition of  $\mathbf{L}_R$ , we have

$$\mathbf{x} = k \cdot \mathbf{U}_R \cdot e^{-\frac{1}{2} \beta \mathbf{A}_R t^2} \cdot \mathbf{U}_R^T \quad (10)$$

Then the dynamic functional correlation is given as

$$\mathbf{f}(t) = \mathbf{x} \cdot \mathbf{x}^T = C e^{-\beta \mathbf{L}_R t^2} \quad (11)$$

where  $C = k^2$  is a constant.

*The determination of  $\mathbf{L}_R$  at resonance.*—The self-organizing interaction of excitation and inhibition between brain regions will lead to resonance with SC at a critical time  $t_{crit}$  where the correlation between  $\mathbf{f}(t)$  and the observed FC will reach a maximum.

Factorizing the FC connectome matrix using eigendecomposition, we obtain,

$$\mathbf{FC} = \mathbf{U}_F \mathbf{A}_F \mathbf{U}_F^{-1} \quad (12)$$

Without loss of generality, we set  $\mathbf{C}$  to 1. To make the correlation between  $\mathbf{f}(t)$  and FC maximized at  $t_{crit}$ , the following two relations should hold, i.e.,  $\mathbf{U}_F \approx \mathbf{U}_R$ ,  $\mathbf{A}_F \approx e^{-\beta \mathbf{A}_R t_{crit}^2}$ . Note that from  $\mathbf{L}_R = \mathbf{D} - \mathbf{W} \circ \mathbf{S}$ , it can be observed that the signs of the elements in  $-\mathbf{L}_R$  are the same as those in the sign matrix  $\mathbf{S}$  except the diagonal entries. Applying Tailor expansion gives

$$\mathbf{f}(t) = e^{-\beta \mathbf{L}_R t^2} \approx \mathbf{I} - \beta \mathbf{L}_R t^2 \quad (13)$$

where  $\mathbf{I}$  denotes the identity matrix. This approximation implies that the signs of the off-diagonal entries in  $\mathbf{f}(t)$  are nearly the same as those in  $\mathbf{S}$ , suggesting that we can make the sign of each elements in matrix  $\mathbf{S}$  equal to those of the corresponding elements in FC. Then  $\mathbf{U}_R$  can be

modeled as the harmonics yielded by the following Laplacian eigendecomposition

$$\mathbf{L}_H = (\mathbf{D}_H - \mathbf{W}_H) \circ \mathbf{S} = \mathbf{U}_H \mathbf{A}_H \mathbf{U}_H^T \quad (14)$$

where  $\mathbf{W}_H$  corresponds to an adjacency matrix with all the elements being 1 excluding the diagonal entries,  $\mathbf{D}_H$  is the degree matrix of  $\mathbf{W}_H$ .

As for  $\mathbf{A}_R$ , previous findings have already shown that the relationship between the eigenvalues of FC,  $\mathbf{A}_F$ , and the Laplacian eigenvalues of SC,  $\mathbf{A}$ , conforms to a negative exponential relation [18, 31], therefore  $\mathbf{A}_R$  can be replaced with  $\mathbf{A}$ .

Taken together, the resonant Laplacian,  $\mathbf{L}_R$ , can be reformulated as the following form when resonance occurs,

$$\mathbf{L}_R = \mathbf{U}_H \mathbf{A} \mathbf{U}_H^T \quad (15)$$

where  $\mathbf{U}_H$  represents the harmonics shaped by the self-organizing interplay of excitation and inhibition between brain regions, while  $\mathbf{A}$  specifies the natural frequencies of SC.

*Connectome dataset.*—The connectome dataset we used was obtained from the Human Connectome Project (HCP —www.humanconnectome.org, S1200 release) [32]. We selected subjects with high-quality fMRI data. Finally, our study consisted of 1038 healthy adults. The whole cerebral cortex was partitioned into 360 regions of interest (ROIs) using HCP-MMP1.0 atlas [33]. The functional connectomes were specified using Pearson's correlation between BOLD time series after data preprocessing. The structural connectomes we used were open source probabilistic connectomes [34], including 1065 subjects, in which the corresponding 1038 subjects were selected. It is worth mentioning that we removed weak connections whose connection strengths are below 0.001. The mean empirical SC and FC connectomes for the first 130 subjects were demonstrated in Fig. S1(a) and (b). For more details, see *SI* Methods and Ref. [34].

*Prediction of resting-state FC.*—As was shown in Eq. (11), the dynamic couplings between brain regions at rest vary in the form of a Gaussian wave regulated by the Laplacian in Eq. (15). Suppose the sign matrix  $\mathbf{S}$  is known,  $C$  can be initially set to be 1, and  $\beta$ , the decay factor, which controls the time width of  $f(t)$ , is experimentally chosen as 0.1, then the theoretical dynamic functional connectivity can be obtained.

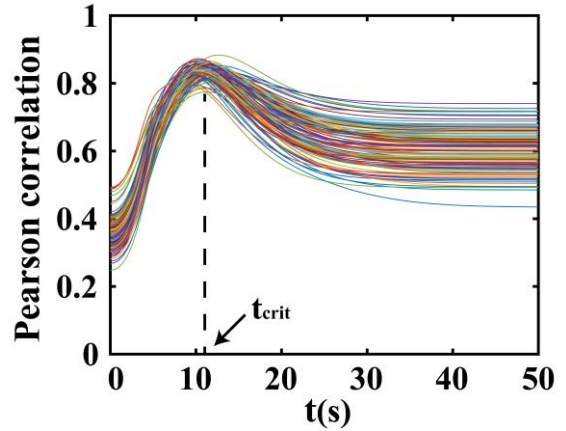


FIG. 1 The evolution of the Pearson correlations with the empirical FC for the first 130 subjects over time ( $p < 1.0 \times 10^{-6}$ ). The maximum correlations arise at  $10.8115 \pm 0.9092$ s.

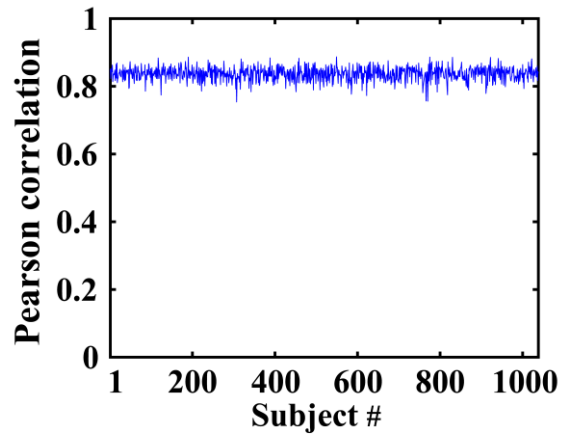
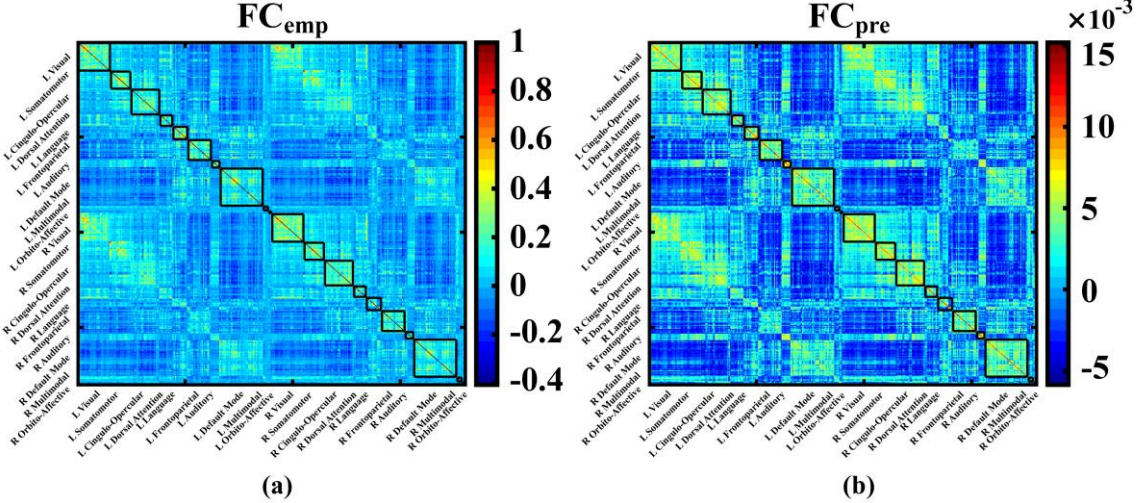


FIG. 2 The maximum Pearson correlation values (characterized by  $f(t)$  at the critical time in Fig. 1) for all the 1038 subjects. The mean correlation is  $0.8366 \pm 0.0198$  ( $p < 1.0 \times 10^{-6}$ )



**FIG. 3** The comparison between the mean predicted RSNs and the mean empirical RSNs for the first 130 subjects. **(a)** The mean empirical RSNs. **(b)** The corresponding mean predicted RSNs. For clearly visualization the brain areas are reordered and organized into 10 RSNs for each hemisphere. See Ref. [34] for more details.

**TABLE I.** The Pearson correlations for each of the 10 predicted RSNs ( $p < 1.0 \times 10^{-6}$ ) (LH—Left Hemisphere; RH—Right Hemisphere)

RSNs	LH	RH
Visual	$0.7913 \pm 0.0545$	$0.7868 \pm 0.0595$
Somatomotor	$0.7563 \pm 0.0679$	$0.7496 \pm 0.0685$
Cingulo-opercular	$0.7374 \pm 0.0428$	$0.7544 \pm 0.0509$
Dorsal attention	$0.8350 \pm 0.0449$	$0.8227 \pm 0.0370$
Language	$0.8508 \pm 0.0380$	$0.8672 \pm 0.0313$
Frontoparietal	$0.8436 \pm 0.0394$	$0.8141 \pm 0.0337$
Auditory	$0.7671 \pm 0.0778$	$0.8030 \pm 0.0463$
Default mode	$0.7398 \pm 0.0420$	$0.7609 \pm 0.0367$
Multimodal	$0.8617 \pm 0.0437$	$0.8553 \pm 0.0503$
Orbito-Affective	$0.9207 \pm 0.0467$	$0.9158 \pm 0.0448$

The performances were assessed for each subject respectively with the Pearson correlation between  $f(t)$  and the empirical FC. Figure 1 shows the evolution of the Pearson correlations for the first 130 subjects over time, respectively. Figure 2 plots the maximum Pearson correlation values (characterized by  $f(t)$  at the critical time) for all the 1038 subjects. It can be seen that very high Pearson correlation values ( $> 0.8$ ) are obtained for almost all the subjects, which significantly exceeds the performance of some

state-of-the-art models using eigen-decomposition [17, 18, 21, 22, 31], including two learning-based approaches [20, 35]. Figure S1 (c) illustrates the mean predicted whole FC patterns of the first 130 subjects, which show strong resemblance to the empirical FC measured with fMRI (Fig. S1 (b)).

*Prediction of 20 resting-state networks (RSNs).*— To show the predictive power of our model, we further perform evaluations on predicting the resting-state networks (RSNs). For each hemisphere of the 180 cortical regions, we extract 10 RSNs [34], namely, visual, somatomotor, cingulo-opercular, dorsal attention, language, frontoparietal, auditory, default mode, multimodal, and orbito-affective. The Pearson correlations for each of the predicted RSNs are listed in Table I. The comparison between the mean predicted RSNs and the mean empirical RSNs for the first 130 subjects are demonstrated in Fig. 3. It can be clearly seen that higher Pearson correlations are also obtained for all the 20 RSNs, showing that the model is able to predict not only the global pattern of FC but also local RSNs.

*Obtaining FC from the model directly.*—It is worth highlighting that the aforementioned predicted FC is evaluated by searching for the maximum Pearson

correlations (see [Fig. 1](#) and [Fig. 2](#)), which draws on the empirical FC to determine the critical time,  $t_{crit}$ , in [Fig. 1](#). Surprisingly, we find that the critical time can also be estimated by computing the Pearson correlation between  $f(t)$  and SC. As shown in [Fig. 4](#), although the Pearson correlations with SC are much lower than with FC, the peak values can also be observed on the correlation curves.

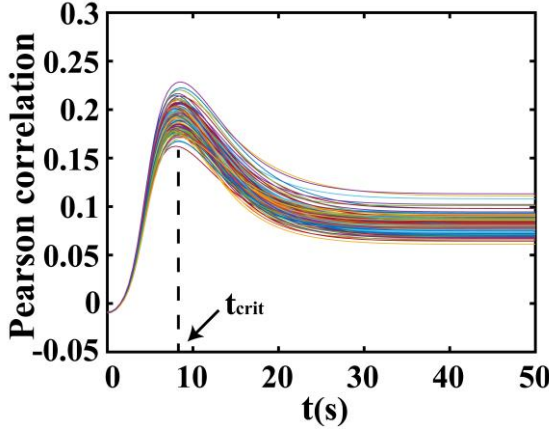


[FIG. 4](#) The evolution of the Pearson correlations with empirical SC for the first 130 subjects over time. The maximum correlations arise at  $8.2888 \pm 0.2844$ s. Note that curves with different colors refer to the Pearson correlations obtained from different subjects ( $p < 1.0 \times 10^{-6}$ ).

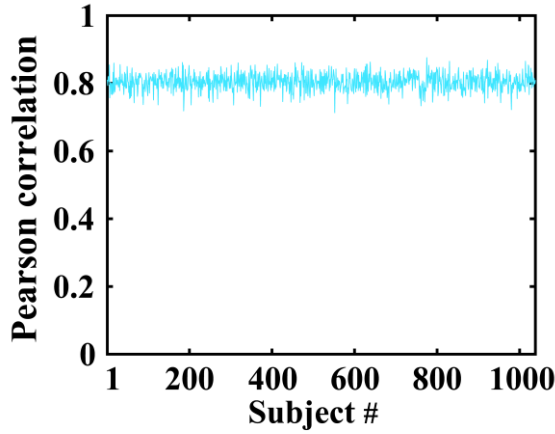


[FIG. 5](#) The maximum Pearson correlation values (characterized by  $f(t)$  at the critical time in [Fig. 4](#)) for all the 1038 subjects. The average correlation is  $0.8038 \pm 0.0247$  ( $p < 1.0 \times 10^{-6}$ )

Therefore, we can estimate  $t_{crit}$  by searching for the maximum Pearson correlations between  $f(t)$  and SC. [Figure 5](#) shows the plot of the maximum Pearson

correlation values obtained at the estimated critical time for all the 1038 subjects. It can be seen that the Pearson correlations for the directly computed FC show slight drop because, for each subject, there is a little variance between the optimal critical time with FC and the estimated critical time with SC.

*Analyzing  $f(t)$  in frequency domain.*—Since  $\int_{-\infty}^{+\infty} e^{-ax^2} dx = \sqrt{\frac{\pi}{a}}$  ( $a > 0$ ), let  $a = \beta L_R$ , we can obtain the Fourier transform of  $f(t)$ ,  $F(\omega)$ , as follows (see [SI](#) for the proof),

$$F(\omega) = \int_{-\infty}^{+\infty} f(t) e^{-j\omega t} dt = \sqrt{\frac{\pi}{\beta L_R}} e^{-\frac{\omega^2}{4\beta L_R}} \quad (16)$$

Given  $\omega = 2\pi f_r$ , where  $f_r$  stands for the real frequency (Hz), then we have

$$F(f_r) = \sqrt{\frac{\pi}{\beta L_R}} e^{-\frac{\pi^2 f_r^2}{\beta L_R}} \quad (17)$$

[Figure 6](#) demonstrates the evolution of the Pearson correlations between  $F(f_r)$  and FC for the first 130 subjects over frequency, respectively. It can be clearly observed that, for every subject, the correlation gets to the maximum at frequency around  $f_r = 0.0529$ Hz, fitting well to the BOLD fluctuations (<0.1Hz).

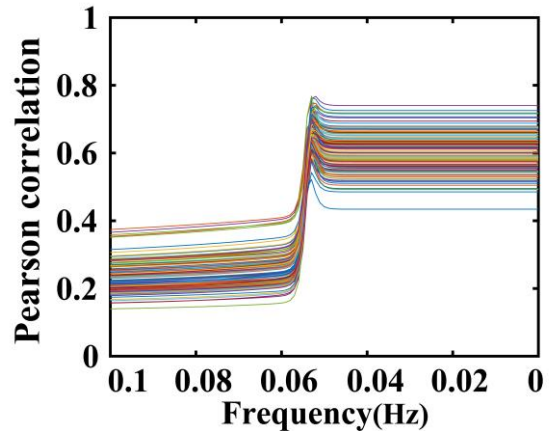


[FIG. 6](#) The evolution of the Pearson correlations with empirical FC for the first 130 subjects over frequency. The maximum correlations arise at frequency around 0.0529Hz ( $p < 1.0 \times 10^{-6}$ ).

Particularly, when  $f_r = 0$ , we can compute the steady state theoretically, i.e.,  $F(0) = \sqrt{\frac{\pi}{\beta L_R}}$  or

$\int_{-\infty}^{+\infty} e^{-\beta L_R t^2} dt = \sqrt{\frac{\pi}{\beta L_R}}$ , indicating that  $f(t)$  will keep constant after resting-state FC arises, from which the Pearson correlations tend to be the same when the fluctuation tapers off (see [Fig. 1](#) and [Fig. 6](#)).

*Conclusion and Outlook.*—Here we propose a new model to describe the spontaneous cortical activity by incorporating the dynamic interactions between neuronal regions into a wave equation. Theoretical solution shows that the dynamic couplings between brain regions fluctuate in the form of Gaussian wave regulated by the harmonics shaped from the interplay between excitation and inhibition, which may lead to resonance with SC at a critical time from which the resting-state FC arises. Crucially, our modeling results reveal that the dynamic coupling of the cortical activity is largely dominated by two fundamental factors pertaining to SC, one is the Laplacian eigenvalues of the underlying anatomical structure, which control the harmonic frequencies of the neural activity signals; the other is the connection type (excitatory or inhibitory) between connections, which shapes the harmonic waves with each frequency components.

Remarkably, the resting-state FC can be theoretically determined from the model given that the structural connection strength and the sign (excitatory or inhibitory) of each connection are known, which produces similar functional patterns with the empirical FC, suggesting that we can directly obtain the resting-state FC from SC using the model. Further, we have also given analysis of our model in frequency domain and find that the predicted resting-state FC really emerges at a low frequency (around 0.0529Hz), which is highly consistent with the BOLD signals measured with fMRI and strongly confirms the significance of our model.

The major limitation remaining in our model is the determination of the connection signs (excitatory or

inhibitory) in SC, which is central to obtaining FC automatically. Although, we are unable to obtain the relevant information due to the inability of the current diffusion imaging and tractography techniques to measure the direction and causality between connections, we firmly believe that this problem will be addressed with the advent of new neuroimaging methods and new modeling approaches in the coming years.

Taken together, the proposed resonance model is able to bring to light how neural activities are coupled and propagate in brain. Particularly, it may give us hope to conjecture whether the same way is carried out in brain during performing cognitive tasks such as learning, memory, as well as decision making [\[36\]](#).

This work is funded by the National Natural Science Foundation of P.R. China (Grant No. 62072468). We thank B. Q. Rosen and E. Halgren for sharing the probabilistic connectome data at <http://zenodo.org/record/4060485>. The rs-fMRI data were provided by the Human Connectome Project, WU-Minn Consortium (Principal Investigators: David Van Essen and Kamil Ugurbil; 1U54MH091657) funded by the 16 NIH Institutes and Centers that support the NIH Blueprint for Neuroscience Research; and by the McDonnell Center for Systems Neuroscience at Washington University.

\* [yjwang@upc.edu.cn](mailto:yjwang@upc.edu.cn)

- [1] M. D. Fox and M. E. Raichle, Spontaneous fluctuations in brain activity observed with functional magnetic resonance imaging, *Nat Rev Neurosci* **8**, 700-711 (2007).
- [2] P. Hagmann, L. Cammoun, X. Gigandet, R. Meuli, C. J. Honey, Van J. Wedeen, and O. Sporns, Mapping the structure core of human cerebral cortex. *PLoS Bio* **16**, e159 (2008).
- [3] E. Bullmore, and O. Sporns, Complex brain networks: graph theoretical analysis of structural and functional systems. *Nat Rev Neurosci* **10**, 186-198 (2009).
- [4] M. Rubinov, and O. Sporns, Complex network measures of brain connectivity: Uses and interpretations. *NeuroImage* **52**, 1059-1069 (2010).

- [5] C. J. Honey, O. Sporns, L. Cammoun, X. Gigandet, J. P. Thiran, R. Meuli, and P. Hagmann, Predicting human resting-state functional connectivity from structural connectivity. *Proc Natl Acad Sci USA* **106**, 2035-2040 (2009).
- [6] J. Goñi, M. P. van den Heuvel, A. Avena-Koenigsberger, N. V. de Mendizabal, R. F. Betzel, A. Griffa, P. Hagmann, B. Corominas-Murtra, J. P. Thiran, and O. Sporns, Resting-brain functional connectivity predicted by analytic measures of network communication. *Proc Natl Acad Sci USA* **111**, 833-838 (2014).
- [7] P. Tewarie, A. Hillebrand, E. van Dellen, M.M. Schoonheim, F. Barkhof, C.H. Polman, C. Beaulieu, G. Gong, B.W. van Dijk, and C.J. Stam, Structural degree predicts functional network connectivity: A multimodal resting-state fMRI and MEG study. *NeuroImage* **97**, 296-307 (2014).
- [8] C. J. Stam, E. C. W. van Straaten, E. Van Dellen, P. Tewarie, and G. Gong, A. Hillebrand, The relation between structural and functional connectivity patterns in complex brain networks. *Int. J. Psychophysiol.* **103**, 149-160 (2016).
- [9] A. Haimovici, E. Tagliazucchi, P. Balenzuela, and D. R. Chialvo, Brain organization into resting state networks emerges at criticality on a model of the human connectome. *Phys Rev Lett.* **110**, 178101(2013).
- [10] Y. Iturria-Mediana, E. J. Canales-Rodríguez, L. Melie-Carcía, P. A. Valdés-Hernández, E. Martínez-Montes, Y. Alemán-Gómez, and J.M . Sánchez-Bornot, Characterizing brain anatomical connections using diffusion weighted MRI and graph theory. *NeuroImage* **36**, 645-660 (2007).
- [11] C. J. Honey, R. Kotter, M. Breakspear, and O. Sporns, Network structure of cerebral cortex shapes functional connectivity on multiple time scale, *Proc Natl Acad Sci USA* **104**, 10240-10245 (2007).
- [12] G. Deco, A. Ponce-Alvarez, D. Mantini D, G. L. Romani, P. Hagmann, and M. Corbetta, Resting-state functional connectivity emerges from structurally and dynamically shaped slow linear fluctuations. *J Neurosci* **33**, 11239-11252 (2013).
- [13] G. Deco, A. R. McIntosh, K. Shen, R. M. Hutchison, R. S. Menon, S. Everling, P. Hagmann, and V. K. Jirsa, Identification of optimal structural connectivity using functional connectivity and neural modeling. *J. Neurosci.* **34**, 7910-7916 (2014).
- [14] X. Chen, and Y. Wang, Exploring the dynamic relation between human brain structural and functional connectivity based on SIS model. *IEEE-CAA J. Automatic.* **5**, 1079-1088 (2018).
- [15] P. A. Robinson, X. Zhao, K. M. Aquino, J. D. Griffiths, S. Sarkar, and G. Mehta-Pandejee, Eigenmodes of brain activity: Neural field theory predictions and comparison with experiment. *Neuroimage* **142**, 79-98 (2016).
- [16] M. Aqil, S. Atasoy, M. L. Kringelbach, and R. Hindriks, Graph neural fields: A framework for spatiotemporal dynamical models on the human connectome. *Plos Comput. Bio.* **17**, e1008310 (2021).
- [17] F. Abdelnour, H. U. Voss, and A. Raj, Network diffusion accurately models the relationship between structural and functional brain connectivity networks. *Neuroimage* **90**, 335-347 (2014).
- [18] F. Abdelnour, M. Dayan, O. Devinsky, T. Thesen, and A. Raj, Functional brain connectivity is predictable from anatomic network's Laplacian eigen-structure. *NeuroImage* **172**, 728-739 (2018).
- [19] P. A. Robinson, S. Sarkar, Grishma. Mehta-Pandejee, J. A. Henderson, Determination of effective brain connectivity from functional connectivity with application to resting state connectivities. *Phys Rev E* **90**, 012707 (2014).
- [20] C. O. Becker, S. Pequito, G. J. Pappas, M. B. Miller, S. T. Grafton, D. S. Bassett, V. M. Preciado, Spectral mapping of brain functional connectivity from diffusion imaging. *Sci Rep* **8**, 1411 (2018).
- [21] S. Deslauriers-Gauthier, M. Zucchelli, M. Frigo, R. Deriche, A unified framework for multimodal structure-function mapping based on eigenmodes. *Med Image Anal* **66**, 101799 (2020).
- [22] P. Tewari, B. Prasse, J. M. Meier, et al., Mapping functional brain networks from the structural connectome: Relating the series expansion and eigenmode approaches. *Neuroimage* **216**, 116805 (2020).
- [23] S. Atasoy, I. Donnelly, and J. Pearson, Human brain networks function in connectome-specific harmonic waves. *Nat Comm* **7**, 10340 (2016).
- [24] S. Atasoy, G. Deco, M. L. Kringelbach, and J. Pearson, Harmonic brain modes: A unifying framework for linking space and time in brain dynamics. *The Neuroscientists* **24**, 277-293 (2017).
- [25] M. G. Preti, D. and Van De Ville, Decoupling of brain function from structure reveals regional behavioral specialization in humans. *Nat Comm* **10**, 4747 (2019).

- [26] Y. Wang, J. Ma, X. Chen, and B. Liu, Accurately modeling the resting brain functional correlations using wave equation with spatiotemporal varying hypergraph Laplacian, *IEEE Trans. Med. Imaging*, online version <https://doi.org/10.1109/TMI.2022.3196007>
- [27] J. S. Isaacson, and M. Scanziani, How inhibition shapes cortical activity. *Neuron* **72**, 231-243 (2011).
- [28] G. Deco, V. Jirsa, A. R. McIntosh, O. Sporns, and R. Kötter, Key role of coupling, delay, and noise in resting brain fluctuations. *Proc Natl Acad Sci USA* **106**, 10302-10307 (2009).
- [29] G. Bi, and M. Poo, Synaptic modifications in cultured hippocampal neurons: Dependence on spiking timing, synaptic strength, and postsynaptic cell type. *The Journal of Neuroscience* **18**, 10464-10472 (1998).
- [30] R. C. O'Reilly, Y. Munakata, M.J. Frank, T. E. Hazy, and Contributors, *Computational Cognitive Neuroscience*, Open Textbook, 4th Edition, 65-77 (2020). URL: <https://CompCogNeuro.org>.
- [31] J. Ma, Y. Wang, B. Liu, and W. Liu, Accurately modeling the human brain functional correlations with hypergraph Laplacian. *Neurocomputing* **428**, 239-247 (2021).
- [32] D. C. Van Essen, K. Ugurbil, E. Auerbach, D. Barch, T. E. J. Behrens, R. Bucholz,..., and WU-Minn HCP Consortium, The Human Connectome Project: a data acquisition perspective. *Neuroimage* **62**, 2222-2231 (2012).
- [33] M. Glasser, T. Coalson, E. Robinson, *et al.*, A multi-modal parcellation of human cerebral cortex. *Nature* **536**, 171–178 (2016).
- [34] B. Q. Rosen and E. Halgren, A whole-cortex probabilistic diffusion tractography connectome. *eNeuro* **8**, 1-21 (2021).
- [35] G. Rosenthal, F. Vasa, A. Griffa, P. Hagmann, E. Amico, J. Goni, G. Avidan, and O. Sporns, Mapping higher-order relations between brain structure and function with embedded vector representations of connectomes. *Nat. Commun.* **9**, 2178 (2018).
- [36] H. J. Park and K. Friston, Structural and functional brain networks: From connections to cognition. *Science* **342**, 1238411 (2013).

# Supplemental Information for “A Resonance Model for Spontaneous Cortical Activity”

Yanjiang Wang<sup>1\*</sup>, Jichao Ma<sup>1</sup>, Jiebin Luo<sup>1</sup>, Xue Chen<sup>2</sup>, Yue Yuan<sup>1</sup>

<sup>1</sup>College of Control Science and Engineering, China University of Petroleum (East China), Qingdao 266580, P. R. China

<sup>2</sup>The Institute for Digital Medicine and Computer-assisted Surgery in Qingdao University, Qingdao University, Qingdao 266071, China

## METHODS

*Data Sources.*—Our data was obtained from the Human Connectome Project (HCP — [www.humanconnectome.org](http://www.humanconnectome.org), S1200 release). We selected subjects with high-quality rfMRI\_REST1\_LR, rfMRI\_REST1\_RL, and Diffusion.bedpostX data. Finally, our study consisted of 1038 adults.

*Scanning Parameters.*—For the structural and diffusion data: All Human Connectome Project imaging data [37] were acquired on a Siemens Skyra 3T scanner with a customized SC72 gradient insert. T1w 3D MPRAGE were acquired with TR=2400ms, TE=2.14ms, TI=1000ms, flip angle=8°, FOV=224x224, 0.7mm isotropic voxel, bandwidth=210Hz/px, iPAT=2, Acquisition time=7:40 (min:sec). Diffusion weighted images were acquired with Spin-echo EPI sequences (b-values=0, 1000, 2000, 3000 s/mm<sup>2</sup> in approximately 90 gradient directions, TR=5520 ms, TE=89.5 ms, flip angle=78°, refocusing flip angle=160°, FOV=210x180 (RO x PE) matrix=168x144 (RO x PE), slice thickness=1.25mm, 111 slices, 1.25mm isotropic voxels, Multiband factor=3, Echo spacing=0.78ms, BW=1488 Hz/Px, Phase partial Fourier 6/8 [38].

For the resting-state fMRI: Sequence: Gradient-echo PLI, TR: 720ms, TE: 33.1ms, flip angle 52 deg, FOV: 208x180mm (RO x PE), Matrix: 104x90 (RO x PE), Slice thickness: 2.0 mm; 72 slices; 2.0 mm isotropic voxels. Multiband factor: 8, Echo spacing:

0.58 ms, BW: 2290 Hz/Px. Resting state data produced 1200 frames per run (time points), of total duration: 14 minutes 33 seconds. For further details, see Ref. [39].

*fMRI Data Preprocessing and Generating Functional Connectome.*—All resting-state fMRI data were minimally preprocessed with echo planar imaging gradient distortion correction, motion correction, field bias correction, spatial transformation and normalization into a common MNI space [40] (Glasser et al. 2013) and artifact removal using independent component analysis (ICA) + FIX [41, 42]. We used dpabi (<http://www.rfmri.org/dpabi>) [43] to remove global signal and estimated functional Connectomes using Pearson’s correlation between time points, the network nodes defined by using HCP-MMP1.0 atlas [44].

*Probabilistic Structural Connectome.*—We used open source probabilistic connectomes [45]. The connectomes was constructed by probabilistic tractography, the nodes also defined by using HCP-MMP1.0 atlas. The probabilistic connectomes have been normalized and symmetric.

## PROOF OF THE SOLUTION OF THE WAVE EQUATION

As described in the main text, the wave equation can be expressed as

$$\frac{\partial^2 \mathbf{x}}{\partial t^2} = \beta^2 \mathbf{L}_R^2 t^2 \mathbf{x} \quad (18)$$

The solution is derived as follows.

$$\text{Assume } \frac{\partial \mathbf{x}}{\partial t} = \boldsymbol{\rho}, \text{ then } \frac{\partial^2 \mathbf{x}}{\partial t^2} = \frac{\partial \boldsymbol{\rho}}{\partial t} = \frac{\partial \boldsymbol{\rho}}{\partial \mathbf{x}} \cdot \frac{\partial \mathbf{x}}{\partial t} = \boldsymbol{\rho} \cdot \frac{\partial \boldsymbol{\rho}}{\partial \mathbf{x}},$$

and then the wave equation can be rewritten as

$$\boldsymbol{\rho} \frac{\partial \boldsymbol{\rho}}{\partial \mathbf{x}} = \beta^2 \mathbf{L}_R^2 t^2 \mathbf{x} \quad (19)$$

i.e.,  $\boldsymbol{\rho} \partial \boldsymbol{\rho} = \beta^2 \mathbf{L}_R^2 t^2 \mathbf{x} \partial \mathbf{x}$ , integrating on both sides gives,

$$\frac{1}{2} \boldsymbol{\rho}^2 = \frac{1}{2} \beta^2 \mathbf{L}_R^2 t^2 \mathbf{x}^2$$

Considering the damping effect during the propagating of neural activity signals, the solution  $\boldsymbol{\rho}$  can be expressed as

$$\boldsymbol{\rho} = -\beta \mathbf{L}_R t \mathbf{x} \quad (20)$$

i.e.,  $\frac{\partial \mathbf{x}}{\partial t} = -\beta \mathbf{L}_R t \mathbf{x}$ , shifting  $\mathbf{x}$  to the left side

and  $t$  to the right side, we have

$$\frac{\partial \mathbf{x}}{\mathbf{x}} = -\beta \mathbf{L}_R t \partial t \quad (21)$$

Integrating on both sides gives

$$\ln(\mathbf{x}) = -\frac{1}{2} \beta \mathbf{L}_R t^2 + k \quad (22)$$

Then we obtain

$$\mathbf{x} = k e^{-\frac{1}{2} \beta \mathbf{L}_R t^2} \quad (23)$$

where  $k$  is a constant.

### PROOF OF THE FOURIER TRANSFORM OF $f(t)$

Since  $\int_{-\infty}^{+\infty} e^{-at^2} dt = \sqrt{\frac{\pi}{a}}$  ( $a > 0$ ), then

$$F(\omega) = \int_{-\infty}^{+\infty} f(t) e^{-j\omega t} dt = \int_{-\infty}^{+\infty} e^{-at^2} e^{-j\omega t} dt$$

$$= \int_{-\infty}^{+\infty} e^{-(at^2 + j\omega t)} dt = \int_{-\infty}^{+\infty} e^{-a\left(t + \frac{j\omega}{2a}\right)^2 - \frac{\omega^2}{4a}} dt$$

$$= e^{-\frac{\omega^2}{4a}} \int_{-\infty}^{+\infty} e^{-\left(\sqrt{at} + \frac{j\omega}{2\sqrt{a}}\right)^2} dt \quad (24)$$

Let  $u = \sqrt{at} + \frac{j\omega}{2\sqrt{a}}$ , then

$$\begin{aligned} F(\omega) &= e^{-\frac{\omega^2}{4a}} \int_{-\infty}^{+\infty} e^{-u^2} \frac{1}{\sqrt{a}} du \\ &= \frac{1}{\sqrt{a}} e^{-\frac{\omega^2}{4a}} \int_{-\infty}^{+\infty} e^{-u^2} du \\ &= \sqrt{\frac{\pi}{a}} e^{-\frac{\omega^2}{4a}} \end{aligned} \quad (25)$$

Let  $a = \beta \mathbf{L}_R$ , we obtain

$$F(\omega) = \sqrt{\frac{\pi}{\beta \mathbf{L}_R}} e^{-\frac{\omega^2}{4\beta \mathbf{L}_R}} \quad (26)$$

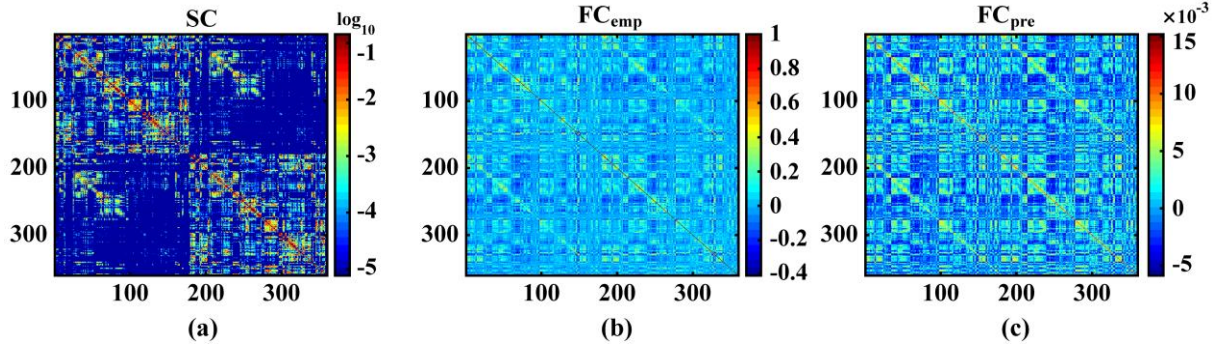


**FIG. S1.** The mean empirical SC, empirical FC, and predicted FC connectomes for the first 130 subjects. **(a)** The mean empirical SC connectome. **(b)** The corresponding mean empirical FC connectome. **(c)** The mean predicted FC connectome. The matrices' elements are arranged such that the upper left quadrant maps the left brain hemisphere, the lower right quadrant maps the right hemisphere, and the off-diagonal quadrants map the interhemispheric connections.

## REFERENCES

- [37] D. C. Van Essen, K. Ugurbil, E. Auerbach, D. Barch, T. E. J. Behrens, R. Bucholz, ..., and WU-Minn HCP Consortium, The Human Connectome Project: a data acquisition perspective. *Neuroimage* **62**, 2222-2231 (2012).
- [38] S. N. Sotiroopoulos, S. Jbabdi, J. Xu, J. L. Andersson, S. Moeller, E. J. Auerbach, ..., and Wu-Minn Hcp Consortium, Advances in diffusion MRI acquisition and processing in the Human Connectome Project. *Neuroimage*, **80**, 125-143 (2013).
- [39] S. M. Smith, C. F. Beckmann, J. Andersson, E. J. Auerbach, J. Bijsterbosch, G. Douaud, ..., and WU-Minn HCP Consortium, Resting-state fMRI in the human connectome project. *Neuroimage*, **80**, 144-168 (2013).
- [40] M. F. Glasser, S. N. Sotiroopoulos, J. A. Wilson, T. S. Coalson, B. Fischl, J. L. Andersson, ..., and Wu-Minn HCP Consortium, The minimal preprocessing pipelines for the Human Connectome Project. *Neuroimage* **80**, 105-124 (2013).
- [41] G. Salimi-Khorshidi, G. Douaud, C. F. Beckmann, M. F. Glasser, L. Griffanti, and S. M. Smith, Automatic denoising of functional MRI data: combining independent component analysis and hierarchical fusion of classifiers. *Neuroimage* **90**, 449-468 (2014).
- [42] L. Griffanti, G. Salimi-Khorshidi, C. F. Beckmann, E. J. Auerbach, G. Douaud, C. E. Sexton, ... and S. M. Smith, ICA-based artefact removal and accelerated fMRI acquisition for improved resting state network imaging. *Neuroimage* **95**, 232-247 (2014).
- [43] C. Yan, X. Wang, X. Zuo, and Y. Zang, DPABI: Data Processing & Analysis for (Resting-State) Brain Imaging. *Neuroinformatics*, **14**, 339-351 (2016).
- [44] M. Glasser, T. Coalson, E. Robinson, *et al.*, A multi-modal parcellation of human cerebral cortex. *Nature* **536**, 171–178 (2016).
- [45] B. Q. Rosen and E. Halgren, A whole-cortex probabilistic diffusion tractography connectome. *eNeuro* **8**, 1-21 (2021).